A 33-Year Timing Solution of the Redback Millisecond Pulsar Terzan 5A

University of Virginia

Department of Astronomy

Alexandra Rosenthal

Under the guidance of: Dr. Scott Ransom

Submitted in Partial Fulfillment of the Requirements for the

BS Astronomy-Physics Major

Date: May 10, 2024

Draft version May 10, 2024
Typeset using LaTeX **modern** style in AASTeX631

A 33-Year Timing Solution of the Redback Millisecond Pulsar Terzan 5A

Alexandra C. Rosenthal[1] and Scott M. Ransom[1,2]

[1] *University of Virginia*
[2] *National Radio Astronomy Observatory*

ABSTRACT

We present a 33.4-year timing solution of the redback pulsar system Terzan 5A (Ter5A). Redback pulsars are a class of millisecond pulsar with relativistic winds that strongly affect a close main sequence companion star. The ionized wind from the pulsar's ablation of its companion delays or completely obscures the regular pulses and perturbs the canonical "perfect" astrophysical clock. Ter5A, also known as B1744−24A or J1748−2446A, has a 11.56 ms pulse period, a $\sim$0.1 $M_\odot$ dwarf companion star, and an orbital period of 1.82 hours. This system displays highly variable eclipsing and orbital perturbations. Using new timing techniques, we have determined a phase connected timing solution for this system over 33 years, the longest ever published for a redback pulsar. We find that the pulsar's spin variability is much larger than most globular cluster pulsars, and we see no evidence of strong correlations between orbital and spin variability of the pulsar. We also find that astrometric timing measurements are likely too strongly contaminated by this variability to be usable. Finally, we measure an orbital period contraction of -2.175$\times10^{-13}$, which is almost certainly the General Relativity-dominated orbital decay of the system.

1. INTRODUCTION

The high stellar density and high rate of gravitational encounters in globular clusters makes them uniquely productive birthplaces for both millisecond pulsars and for exotic compact binaries. Globular clusters produce orders of magnitude more of these systems per unit mass than the galactic disk (Ransom 2008). So far, astronomers have identified 316 pulsars in 41 globular clusters[1]. As pulsar searches with new and more sensitive telescopes continue, that number will only increase. The interactions between pulsars and cluster stars add additional accelerations to the pulsar that can impact both the spin and orbital parameters (Prager et al. 2017). Though these effects mean that globular cluster pulsars are not useful for certain high-precision timing applications, such as probing the nHz gravitational wave background, the sheer number of cluster pulsars provides a set of data with which one can probe physics ranging from cluster dynamics (Phinney 1993), cluster gas properties (Freire et al. 2001;

[1] https://www3.mpifr-bonn.mpg.de/staff/pfreire/GCpsr.html

Prager et al. 2017), general relativity (Jacoby et al. 2006), and the neutron star equation of state (Homan et al. 2023).

"Spider" pulsars are one subset of the exotic and complex interacting binaries found in globular clusters. In these systems, the relativistic winds from the neutron star ablate away the outer layers of a very close companion star. It is important to note that this mechanism is separate from Roche lobe overflow: in spider pulsar systems, the ablated material may fall onto the pulsar or be ejected from the system entirely. These spider pulsar systems are further subdivided into black widow and redback systems, so named because they "eat" their companions. The subdivision distinguishes between the type of companion and compactness of the binary. Black widow systems typically have lower mass companions ($M_c \ll 0.1\,M_\odot$), and redback systems have higher mass ($M_c \gtrsim 0.1\,M_\odot$) companions (Chen et al. 2013). This paper focuses on one such redback system: Ter5A.

Ter5A is one of the most compact redback systems known. It is also the first redback system detected (Lyne et al. 1990; D.J. Nice 1990), and it is the brightest of the 49 confirmed millisecond pulsars in Terzan 5 (Martsen et al. 2022; Padmanabh et al. 2024). The dense cluster introduces higher-order accelerations to the pulsar beyond the standard spindown over time. There are two timing complications to this system: accelerations from the globular cluster and its stars, and issues from Ter5A's companion. Accounting for the former is a well-documented process (e.g. Prager et al. 2017), but accounting for the latter is difficult on long timing baselines since the orbital parameters are also changing with time. Without such timing methods, redback timing has only been attempted on shorter time spans (Lyne et al. 1990; Nice et al. 2000; Ghosh et al. 2024). Ter5A's companion is a $\sim 0.1\,M_\odot$ star. The system's orbital period is just 1.82 hours, and it is so close to Ter5A that the relativistic winds from the pulsar ablate and evaporate it. The ionized wind blown off the companion produces an eclipse, usually around phase 0.25 of the orbit (i.e. superior conjunction), though the pulsar has been observed to disappear entirely for hours at a time. Additional eclipse-like disappearances at different orbital phases have also been observed. The irregular nature of the gas introduces irregular timing disparities around the eclipse, and the irregular nature of the eclipse itself has made systematic timing prohibitively difficult. Until now, the eclipse and its effects have prevented long-term timing of the system, though the notion of accommodating changing parameters over time has been used to time the system on shorter timing baselines (Nice et al. 2000; Bilous et al. 2011).

Using ∼20 years of archival Green Bank Telescope (GBT) data, and an additional ∼10 years of Very Large Array (VLA) and Green Bank 140-foot data provided by David Nice and Stephen Thorsett, as well as the programs `PINT`[2], `tempo`[3], and a new piecewise continuous binary timing model (O'Neill et al, in prep), we have removed the eclipse and other orbital variability and found a long-term timing solution of this system and tracked its evolution over 33.4 years. This is the longest timing solution for a redback system ever produced.

[2] https://github.com/nanograv/PINT
[3] https://tempo.sourceforge.net/

2. OBSERVATIONS AND METHODOLOGY

Ter5A was observed on 273 days spanning MJDs 47965−60144 (i.e. 1990.2−2023.5). The majority of observations were made between MJDs 53193−60144 (i.e. 2004.5−2023.5) with the Green Bank Telescope (GBT) with the 820 MHz, L-band (1.0-1.8 GHz), and S-band (1.6-2.5 GHz) receivers. The raw data was folded modulo the predicted spin period and integrated over 1 minute intervals to recover the pulse times of arrival (TOAs). Over the span of this dataset, the GBT backend processing system changed from SPIGOT to GUPPI to VEGAS. The SPIGOT observations are described in Ransom et al. (2005). The GUPPI and VEGAS observations, which differ from the earlier observations as coherent dedispersion was used, are described in Martsen et al. (2022). Prior to MJD 53193, most of the TOAs are a combination of Very Large Array (VLA) 1660 MHz data, Green Bank 140 ft 800 MHz and L-band data taken from 1990−1999, and several early GBT observations between 2000−2004. Details on these older TOAs can be found in (Nice et al. 2000; Nice & Thorsett 1992a). We also incorporate data from the Parkes Radio Telescope (Parkes) taken on four days between MJDs 50800−52000 at L-band in a couple different modes. Finally, we incorporate 98 observations of Green Bank 140 ft telescope data at multiple frequencies in the UHF and L-bands taken between MJDs 47966−51363. This information is tabulated in Table 1. We note that observations prior to 2004 were available only in pre-processed TOA format and so had been processed slightly differently and using different pulse templates from the later data. Those earlier datasets therefore require systematic timing offsets between themselves and the latter GBT data (i.e. `JUMP`s).

Before proceeding with any kind of science, the effects of the eclipse had to be removed from the observations, as the ionized gas can cause the measured pulses to be delayed by an unpredictable amount of time. To remove these effects, we cut all TOAs corresponding to an orbital phase between 0.0 and 0.5, where the pulsar was most likely to be eclipsed. We further manually inspected the data to remove any remaining effects of the eclipse. On average, the timing precision of the modern GBT data were much better, allowing for a further error restriction by cutting all TOAs whose formal TOA errors were greater than 7 μs. A summary of the cleaned observations is presented in Table 1.

Figure 1 shows an example of what eclipses can look like in the timing data on a good day (i.e. when the pulsations were basically visible at all orbital phases) and what the timing residuals look like after removing TOAs based on our criteria. As the pulsar moves behind a clump of gas — and note that for the observation in Figure 1 there are two distinct clumps per orbital period, a fairly uncommon occurrence — this gas increases the effective dispersion measure causing pulse delays. These delays do not have the same shape from observation to observation, nor are there even the same number of "eclipses" per orbit from observation to observation. This is one of the reasons long term timing of this system has been prohibitively difficult prior to now.

Fitting these data required some subtle tricks due to the size of the dataset relative to what `PINT` can process when using the piecewise binary timing model with many different

Observatory	Number of TOAs	Frequency (MHz)	Median Error (μs)	Dates (MJD)
GBT	12901	820−2166	87.2	52466−60144
Green Bank 140'	1073	670−1600	237	47966−15363
Parkes	629	1316−1454	246	50800−52000
VLA	699	1667	111	48190−50975

Table 1: Summary of observational data.

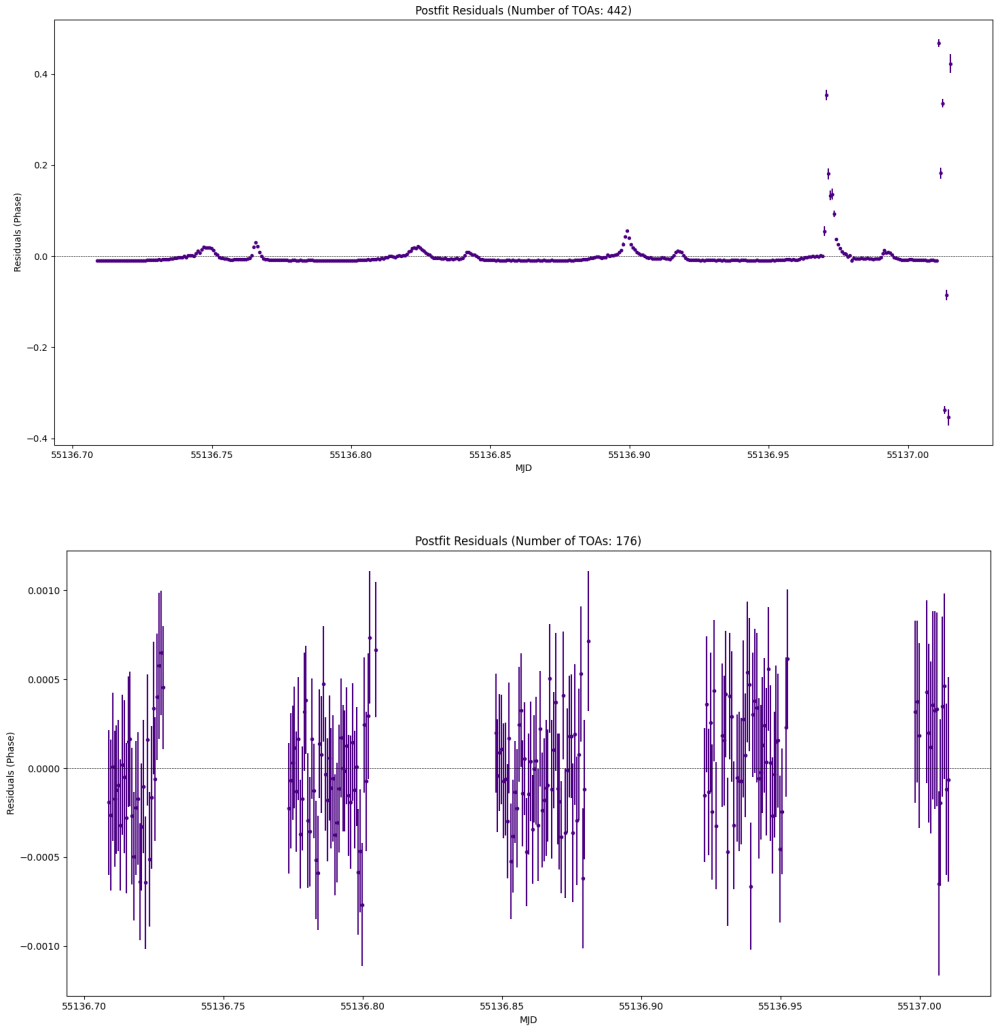

Figure 1: Timing residuals from a day when the pulsations were mostly visible throughout the orbit before cleaning (top) and after cleaning (bottom). These data span four orbits. Note that there are two eclipse-like episodes per orbital period and their shapes do not resemble each other; both the nature and timing of the eclipses are irregular due to the irregularity with which gas is blown off the companion.

piecewise segments and many thousands of TOAs. We fit timing parameters through a bootstrapping process of guess, fit, re-fit the guessed parameter, and fit again. The overview of that process is as follows: 1) we determined orbital phases for each observation, 2) we phase-connected overlapping two-year chunks of data, 3) we verified that the number of pulse rotations between each TOA in the overlapping sections were identical for each section and finally we 4) joined all the sections together using the now known (see step 3) rotational counts between all the TOAs.

In order to fit a long-term timing solution to our several hundred observations, we first sought to phase-connect the data. Phase-connection here means successfully tracking every rotation of the pulsar. Much of the initial processing work was done with `spider_twister`[4]. We generated a "T0" value for each observation using Eqn 1 (see section 3.2). T0 is generally a measure of the precise time of the periastron of the orbit, but for a very nearly circular system such as this one, where we have defined the eccentricity to be zero, T0 is taken to be the time in MJD that the pulsar crosses the plane of the sky moving away from the observer, which is also known as the time of the ascending node. We use this value to track the orbital variation of the system over time.

After generating T0 values, we sorted the observations into two-year pieces that overlapped with each other by approximately six months. Then we fit the spin frequency and spin frequency derivative to these pieces. We additionally manually fit for the `JUMPs` between datasets as un-fit systematics (i.e. timing noise) in the data prevented fitting them accurately alongside other long-term free parameters. We then assigned pulse numbers over the entire dataset, using the overlapping portions to verify phase connection, and then fit the long-term parameters: orbital period, spin frequency, spin frequency derivatives one through five, dispersion measure, and dispersion measure derivative. While this described the long-term orbital variations well, it poorly described individual observations: inspection of individual days revealed sinusoidal residuals with the same period as the orbit, indicating an incorrect T0 value.

In order to nail down the short-term orbital variations of the redback system within the long-term solution, we grouped observations within two weeks of each other into a single fitting range, as over two weeks the periastron of the orbit should not change significantly, and fit a T0 value to replace the predicted value. We measured an orbital period derivative for the system from the deviations between predicted and observed T0s. The ultimate result is a phase-connected solution with well-behaved TOAs in individual observations.

Final refinements to the solution involved testing and implementing additional new timing techniques to reduce the number of TOAs and effectively isolate the pulsar. We used `PINT` and the precisely known T0, P_b, and $\dot{P}_b$ values to subtract off the timing delays from the binary orbit, resulting in a much simpler dataset: an "isolated" pulsar with far fewer parameters to fit. We also condensed each observation into just a few representative and weighted

[4] https://github.com/alex88ridolfi/SPIDER_TWISTER

TOAs, which condensed roughly 15,000 TOAs to just a few hundred. As fitting programs are $O(N^3)$, this was critical to improving quality and runtime of fit by reducing the amount of data the programs had to process, and allowed us to fit for position and proper motion. This simplifying and isolating technique, which effectively de-couples the orbital variations from the long-term spin behavior of the pulsar, worked extremely well and is likely to be useful in other long-term redback timing efforts.

Ultimately we used VLA positions rather than fitting for position and the GAIA measured proper motion for our final fit (see Section 3.4 for more details). The long-term timing parameters are presented at the end of this work.

3. RESULTS

3.1. *Frequency Derivatives and Noise Modeling*

We fit the data through five spin frequency derivatives. Figure 2 shows the evolution of fit with successive derivatives. All plots shown have been fit for position, proper motion, dispersion measure, dispersion measure derivative, frequency, and the number of frequency derivatives indicated. We manually fit `JUMPs` between datasets as fitting for them with other long-term free parameters did not work; conflation with other un-fit systematics (i.e. timing noise) prohibited accurate `JUMP` fits. The data in these plots have also been simplified to a few weighted representative TOAs per day. There is an abrupt feature around the year 2000 (around MJD 51700). This is noted in Nice et al. (2000) and corroborated by our observations. The phase connection of our data suggests this feature is real and corresponds to some physical change in the system.

We measure a spin frequency derivative (i.e. F1) of $1.3340(36)\times10^{-16}\,\mathrm{Hz\,s^{-1}}$. This positive value is consistent with other measured values (e.g. Lyne et al. 1990; Nice & Thorsett 1992b; Prager et al. 2017). The positive first frequency derivative is not attributed to the intrinsic spin-down rate of the pulsar, which must be negative, but likely to the globular cluster accelerating the pulsar toward the observer given the pulsar's likely location on the back side of the cluster. There are additional mechanisms that contribute to apparent positive F1 values, and they usually affect the orbit and spin equally. We discuss this in the next two sections.

3.2. *Orbital variations*

In the absence of external effects, such as that of accelerations from the globular cluster, tidal effects in the bloated companion star, gravitational wave radiation from the compact orbit, and mass transfer or loss from the companion, we can expect T0 will evolve according to

$$T0 = T0_0 + n \times P_{orb} \tag{1}$$

where $T0_0$ is some measured T0, n is the number of orbits that have elapsed between $T0_0$ and T0, and P_{orb} is the orbital period of the binary (1.82 hours). When we compare our measured T0 values with those predicted by this equation, we find that the measured values

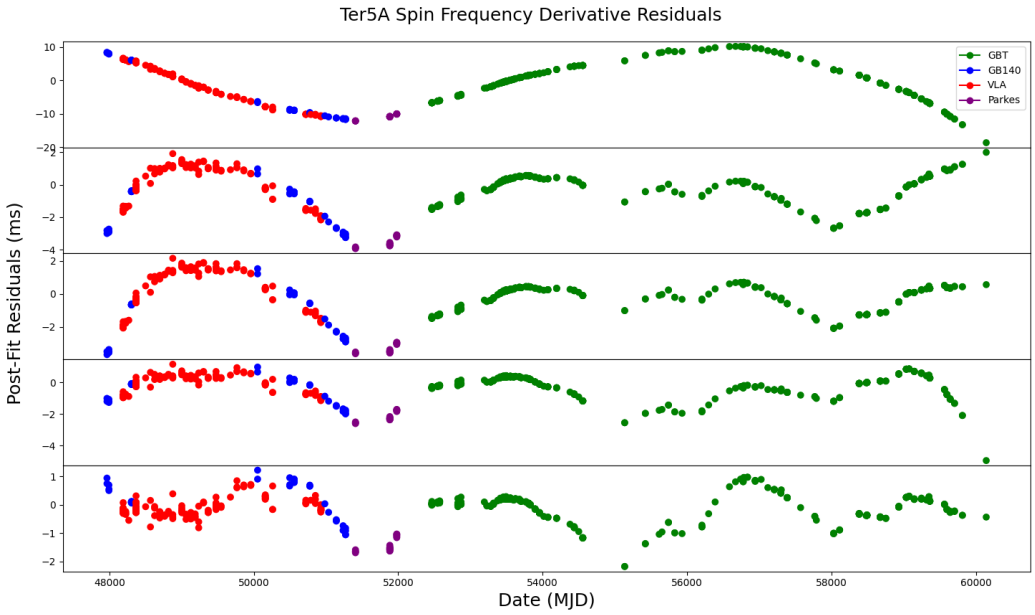

Figure 2: The timing residuals of Ter5A with F0 and F1 (i.e. spin frequency and spin frequency derivative) fit (top), and with increasing numbers of spin frequency derivatives fit, up to and including F5 (bottom). Note the decreasing range covered by the y-axes in each case, showing nominally better fits. Strong systematic trends still remain in the residuals. These can be fit with noise modelling in future work.

vary in a random walk pattern across roughly eleven seconds, as shown in Figure 3. There is an apparent quadratic trend corresponding to the orbital period derivative ($\dot{P_{orb}}$). Adjusting for the effects of $\dot{P_{orb}}$, as described in the next section, results in a random walk spanning plus or minus several seconds, also shown in Figure 3.

We also performed a Gaussian Process Regression on the measured T0 values (see Figure 3) to estimate how smooth the variations might be in time and to better estimate T0 values on days where it wasn't well measured.

3.3. *Orbital Period Derivative*

The predicted $\dot{P}_{orb}$ due to gravitational wave emission is given by Stairs (2003) as

$$\dot{P}_b = -\frac{192\pi}{5}\left(\frac{P_b}{2\pi}\right)^{-5/3}\left(1+\frac{73}{24}e^2+\frac{37}{96}e^4\right)(1-e^2)^{-7/2}\,T_\odot^{5/3}\,m_1\,m_2\,M^{-1/3}, \tag{2}$$

where e is the eccentricity, P_b is the orbital period, M is the total mass of the system, and $T_\odot \equiv GM_\odot/c^3 = 4.925490947\,\mu$s. For Ter5A, the eccentricity is zero, simplifying Eqn 2 to

$$\dot{P}_b = -\frac{192\pi}{5}\left(\frac{P_b}{2\pi}\right)^{-5/3} T_\odot^{5/3}\,m_1\,m_2\,M^{-1/3}. \tag{3}$$

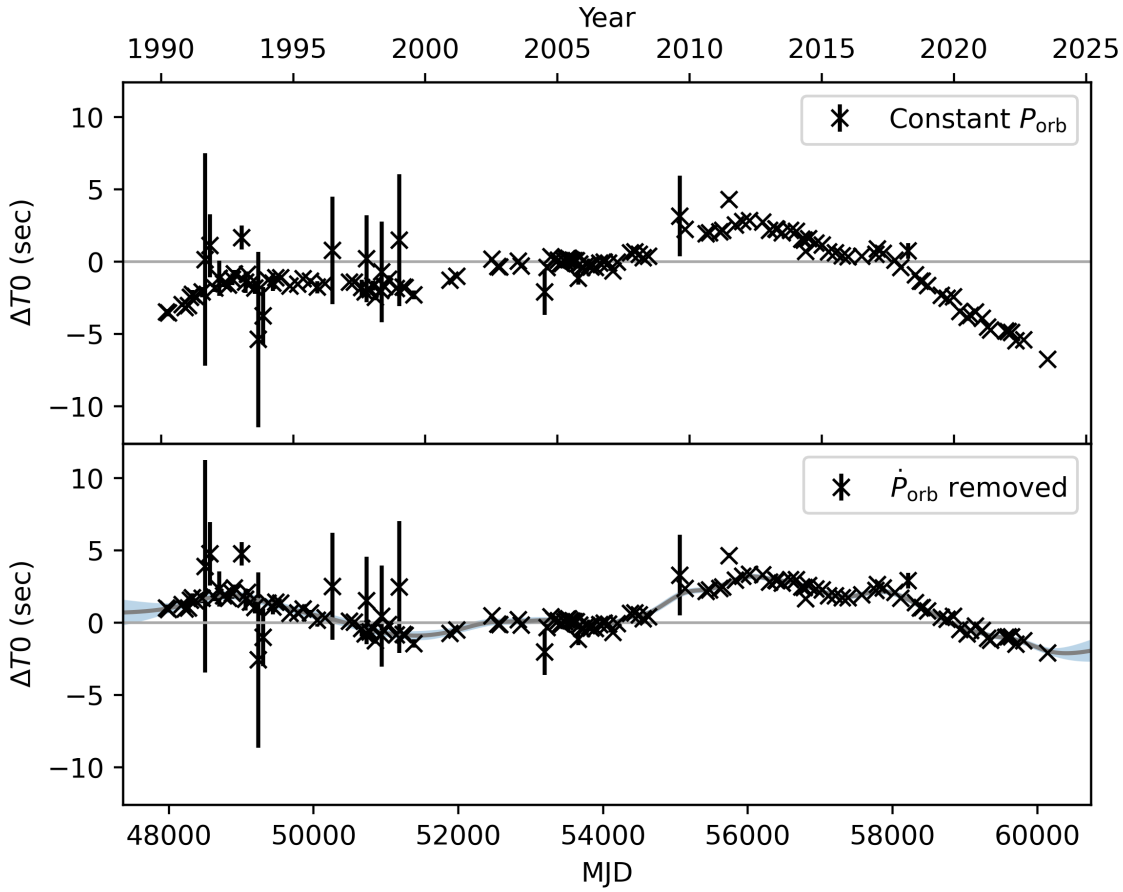

Figure 3: Time of ascending node or periastron passage (T0) deviations over time for Ter5A assuming a constant orbital period (top) and with the best-fit $\dot{P}_{\rm orb}$ removed (bottom). The bottom plot also shows a gaussian process regression to the measured T0 values.

The observed pulsar spin-down to spin period ratio $\frac{\dot{P}}{P}_{obs}$ is given by

$$\frac{\dot{P}}{P}_{obs} = \frac{\dot{P}}{P}_{int} + S + \frac{A_{GC}}{c} + \frac{A_{gal}}{c}, \tag{4}$$

where $\frac{\dot{P}}{P}_{int}$ is the intrinsic spin-down rate of the pulsar, S is the Shklovskii effect (which for this system is negligible), $\frac{A_{GC}}{c}$ is the contribution due to acceleration of the pulsar by the globular cluster, and $\frac{A_{gal}}{c}$ is the contribution due to the acceleration of the pulsar by the Galactic gravitational potential. We note that the error on the $\frac{A_{gal}}{c}$ term may be up to a factor of two. Assuming a reasonable age (5.0×10^9 years, within a factor of ten) and magnetic field strength (7×10^8 Gauss, again within a factor of ten or so) of the pulsar by comparing its period and period derivative to a $P - \dot{P}$ diagram, we can predict $\frac{\dot{P}}{P}_{int}$. $\frac{A_{gal}}{c}$ can be estimated from models based on known distance to the pulsar. Solving for the only remaining unknown, we find $\frac{A_{GC}}{c}$ (the dominating term since the pulsar is observed to have

Component	Value
$\frac{\dot{P}}{P}_{spin}$	$-1.586 \times 10^{-18} s^{-1}$
$\frac{\dot{P}}{P}_{gal}$	$3.579 \times 10^{-18} s^{-1}$
$\frac{\dot{P}}{P}_{S}$	$4.650 \times 10^{-19} s^{-1}$
$\frac{\dot{P}}{P}_{clust}$ (predicted)	$-4.500 \times 10^{-18} s^{-1}$
$\frac{\dot{P}}{P}_{GR}$	$-2.851 \times 10^{-17} s^{-1}$
$\frac{\dot{P}_b}{P_b}$	$-3.328 \times 10^{-17} \pm 0 s^{-1}$
Predicted $\dot{P}_b$	$-2.127 \times 10^{-13} s^{-1}$
Measured $\dot{P}_b$	$-2.175 \times 10^{-13} \pm 0 s^{-1}$

Table 2: Preliminary breakdown of orbital period derivative contributions according to the model of a $1.5\,M_\odot$ pulsar in an $i = 90\,$deg inclined system. Errors on individual components vary significantly and have not been well constrained, but prediction and measurement are both likely precise to two significant figures.

a positive frequency derivative) to be $-4.500 \times 10^{-18} s^{-1}$. We can then use this to consider the orbital period derivative accelerations:

$$\frac{\dot{P}_b}{P_b}_{obs} = S + \frac{A_{GC}}{c} + \frac{A_{gal}}{c} + \frac{A_{GR}}{c} \tag{5}$$

Assuming a $1.5\,M_\odot$ pulsar in an $i = 90\,$deg inclined system, we predict the rate of contraction due to general relativity to be on the order of -2.1×10^{-13}, and from fitting we measure a rate of $-2.175(5) \times 10^{-13}$. In short, this is an edge-on system with an average mass millisecond pulsar, and there are not significant contributors to the contraction of the system in addition to those already listed. The calculations of various components of the system's acceleration are presented in Table 2. General relativisticcontraction of the orbit due to the emission of gravitational radiation is the dominant term in this system.

3.4. *Position and Proper Motion*

Our measured right ascension and declination are tabulated with other reported values in Table 3 and plotted in Figure 4. Taken at face value, our positions are the most precise and we note a massive change in the measured declination. However, these values are erroneous, and entirely inconsistent with VLA data (Fruchter & Goss 2000; Urquhart et al. 2020). Long-term timing noise overpowers the position signal.

Furthermore, we measure a proper motion in the RA direction of $-1.53(11)$ mas/yr and in the Dec direction of $-24.5(3.2)\,$mas/yr. While the RA-proper motion (PMRA) isn't too inconsistent, the declination-proper motion (PMDEC) radically differs from the GAIA measured proper motion of the Terzan 5 cluster of $-1.989 \pm 0.068\,$mas/yr in the RA direction and $-5.243 \pm 0.066\,$mas/yr in the declination direction (Vasiliev & Baumgardt (2021)). This pulsar is very close to the ecliptic plane (ecliptic latitude of $-1.36\,$deg), which makes timing measurements of declination significantly harder due to projection effects.

Paper	Right Ascension	Declination	Observation Date (MJD)
Lyne et al. (1990)	17h48m02.25849(300)s	-24d46m37.1347(4000)s	47992
Nice & Thorsett (1992b)	17h48m02.2534(11)s	-24d46m37.7(5)s	48270
Fruchter & Goss (2000)	17h48m02.2685(50)s	-24d46m37.23(5)s	47892 (approx)
Urquhart et al. (2020)	17:48:02.249(50)	-24:46:37.65(10)	56658 (est)
This Work	17:48:02.25185138(2)	-24:46:39.215100(7)	54054

Table 3: J2000 measured positions of Ter5A by work. Note the errors on this work are far too precise; these are the nominal timing errors but they are swamped by other systematics.

While in principle these results could suggest that Ter5A is not actually a cluster member, this is highly unlikely. The observed positive frequency derivative is almost certainly indicative of cluster membership. Our timing-measured proper motion is inconsistent with the corresponding orbital dynamics. If Ter5A is indeed a cluster member, its elliptical orbit about the cluster core would never take it on such a trajectory. It cannot even be sensibly ejected in this direction. See Figure 5 for a map. Furthermore, setting the proper motion of our system to that of the cluster slightly improves the fit. While short timing baseline observations appear to be successful in timing the position of this system, over longer baselines the long-term timing noise becomes highly covariant with the proper motion signal.

As a result, we take our timing solution as having the position determined by the A-array VLA (Urquhart et al. 2020) and the proper motion measured by GAIA (Vasiliev & Baumgardt 2021). These are the parameters that produced the residuals in Figure 2, and they are smoother than those with our measured proper motion.

4. CONCLUSIONS & FUTURE WORK

We have found a 33.4-year timing solution for the eclipsing millisecond pulsar Terzan 5A, the longest for any redback system. We have tracked the variations in the orbit over time, and even after fitting through five spin frequency derivatives we see strong systematic residuals. This timing noise could be caused by torques on the pulsar due to infalling matter, or by other cluster effects.

We measured the orbital decay of the system over time and found it consistent with GR predictions for a pulsar of $1.5\,M_\odot$, a companion of mass $0.1\,M_\odot$, and a highly-inclined orbit. This also serves as a basic mass measurement, and we conclude that Ter5A is a fairly standard-mass millisecond pulsar. General relativity is the dominant effect in the measured orbital period derivative, which constrains the magnitude of tidal effects in this system.

We could not use timing to determine the position or proper motion of the system because over long-term timing baselines noise overtakes the timing signals of these parameters. However, we successfully used novel timing methods such as bootstrapping parameter-fitting, employing a continuous binary piecewise model, using precise binary values to remove orbital motion of the pulsar and effectively isolate it, and reducing observations to just a few representative TOAs per day, to track this system over a long-term timing baseline.

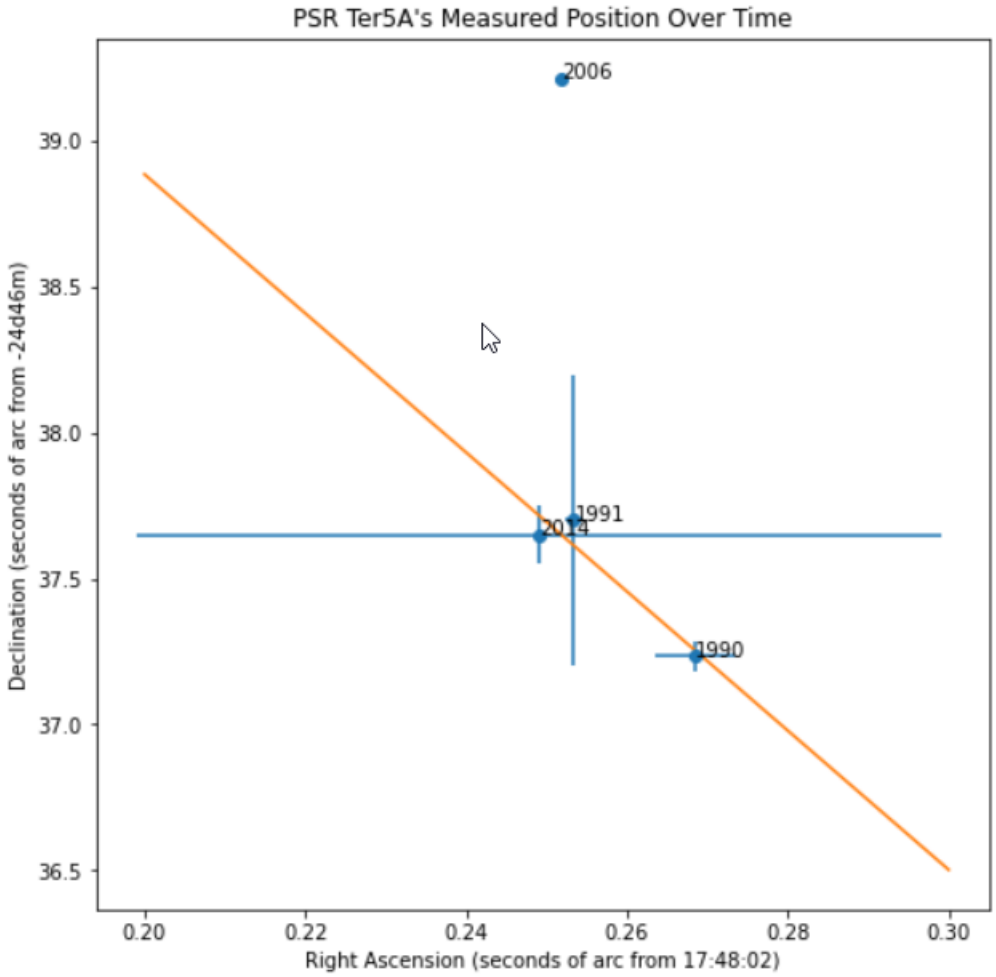

Figure 4: The positions of Ter5A as reported in various works in 3, with the year they are referenced to. Two measurements were from 1990 (see 3, but only the more precise of the two (Fruchter & Goss 2000) is represented on this plot. The 2006 point is our work, which has no error bars as we have formal statistical errors that are tiny, but they are totally swamped by systematic errors due to covariance with timing noise. The orange line is the best fit line of these positions, excluding the 2006 point. We note that careful future examination will be required to make any accurate proper motion measurements.

Possible directions for future work include using our model and all TOAs, including those affected by the eclipse, to probe the immediate environment of Ter5A and examine the companion and the gas blown off it. The model functionality that allowed us to fit for varying T0s will be useful for measuring time-variable DMs. Also, the torque on the pulsar can be calculated and compared to wind-based accretion models as well as the precession of the system predicted in Nice et al. (2000). Investigating the systematics in the spin frequency derivative residuals could reveal more about the source of the timing noise, e.g. companion

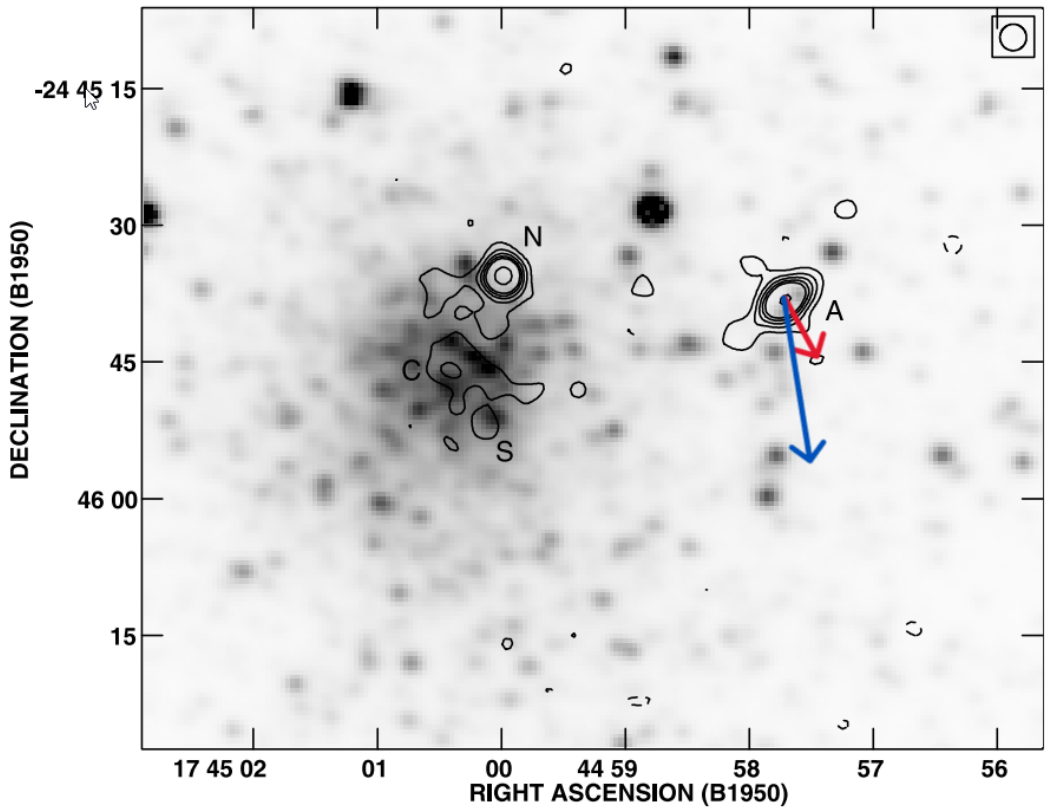

Figure 5: An I-band (optical/IR) backdrop image with L-band radio observations of Terzan 5A and its cluster. Figure modified from Fruchter & Goss (2000). The cluster is noted in the black; Ter5A is denoted with an A. The red arrow indicates the proper motion of the cluster, and the blue arrow indicates our measured proper motion. These vectors are only to scale in relative length and orientation, and not in absolute magnitude. Our measured value is inconsistent with both an elliptical orbit about the cluster and any sensible ejection.

effects, cluster effects, or infalling gas effects. Futhermore, noise modeling could reduce or remove these systematics.

REFERENCES

Bilous, A. V., Ransom, S. M., & Nice, D. J. 2011, in American Institute of Physics Conference Series, Vol. 1357, Radio Pulsars: An Astrophysical Key to Unlock the Secrets of the Universe, ed. M. Burgay, N. D'Amico, P. Esposito, A. Pellizzoni, & A. Possenti (AIP), 140–141, doi: 10.1063/1.3615100

Chen, H.-L., Chen, X., Tauris, T. M., & Han, Z. 2013, The Astrophysical Journal, 775, 27, doi: 10.1088/0004-637x/775/1/27

D.J. Nice, S.E. Thorsett, J. T. A. F. 1990, The Astrophysical Journal Letters, 361, L61, doi: 10.1086/185827

Freire, P. C., Kramer, M., Lyne, A. G., et al. 2001, ApJL, 557, L105, doi: 10.1086/323248

Fruchter, A. S., & Goss, W. M. 2000, ApJ, 536, 865, doi: 10.1086/308948

Ghosh, A., Bhattacharyya, B., Lyne, A., et al. 2024, ApJ, 965, 64, doi: 10.3847/1538-4357/ad31ab

Homan, J., Arzoumanian, Z., Gendreau, K. C., et al. 2023, The Astronomer's Telegram, 15957, 1

Jacoby, B. A., Cameron, P. B., Jenet, F. A., et al. 2006, ApJL, 644, L113, doi: 10.1086/505742

Lyne, A. G., Manchester, R. N., D'Amico, N., et al. 1990, Nature, 347, 650, doi: 10.1038/347650a0

Martsen, A. R., Ransom, S. M., DeCesar, M. E., et al. 2022, ApJ, 941, 22, doi: 10.3847/1538-4357/aca156

Nice, D. J., Arzoumanian, Z., & Thorsett, S. E. 2000, in Astronomical Society of the Pacific Conference Series, Vol. 202, IAU Colloq. 177: Pulsar Astronomy - 2000 and Beyond, ed. M. Kramer, N. Wex, & R. Wielebinski, 67, doi: 10.48550/arXiv.astro-ph/9911211

Nice, D. J., & Thorsett, S. E. 1992a, ApJ, 397, 249, doi: 10.1086/171784

—. 1992b, ApJ, 397, 249, doi: 10.1086/171784

Padmanabh, P. V., Ransom, S. M., Freire, P. C. C., et al. 2024, arXiv e-prints, arXiv:2403.17799, doi: 10.48550/arXiv.2403.17799

Phinney, E. S. 1993, in Astronomical Society of the Pacific Conference Series, Vol. 50, Structure and Dynamics of Globular Clusters, ed. S. G. Djorgovski & G. Meylan, 141

Prager, B. J., Ransom, S. M., Freire, P. C. C., et al. 2017, ApJ, 845, 148, doi: 10.3847/1538-4357/aa7ed7

Ransom, S. M. 2008, in Dynamical Evolution of Dense Stellar Systems, ed. E. Vesperini, M. Giersz, & A. Sills, Vol. 246, 291–300, doi: 10.1017/S1743921308015810

Ransom, S. M., Hessels, J. W. T., Stairs, I. H., et al. 2005, Science, 307, 892, doi: 10.1126/science.1108632

Stairs, I. H. 2003, Living Reviews in Relativity, 6, doi: 10.12942/lrr-2003-5

Urquhart, R., Bahramian, A., Strader, J., et al. 2020, ApJ, 904, 147, doi: 10.3847/1538-4357/abb6fc

Vasiliev, E., & Baumgardt, H. 2021, MNRAS, 505, 5978, doi: 10.1093/mnras/stab1475

Table 4: Parameters for PSR 1748-2446A

Dataset and model summary	
Pulsar name	1748−2446A
MJD range	47965—60144
Data span (yr)	33.34
Number of TOAs	15302
TOA paradigm	Narrowband
Solar system ephemeris	DE440
Timescale	TT(BIPM2019)
Time unit	TDB
Time ephemeris	FB90
Binary model	BT_piecewise
Number of JUMPs	6
Fit summary	
Number of free parameters	13
Fitting method	WLS
RMS TOA residuals (μs)	1230.26
χ^2	769094.33
Reduced χ^2	50.31
Measured Quantities	
RAJ, Right ascension (J2000) ($^{\mathrm{h}}$)	17.80062551(2)
DECJ, Declination (J2000) ($^\circ$)	−24.777588(7)
PMRA, Proper motion in RA ($\frac{\mathrm{mas}}{\mathrm{yr}}$)	−1.5(1)
PMDEC, Proper motion in DEC ($\frac{\mathrm{mas}}{\mathrm{yr}}$)	−25(3)
F0, Spin-frequency (Hz)	86.481636911965(2)
F1, Spin-frequency derivative 1 ($\frac{\mathrm{Hz}}{\mathrm{s}}$)	$1.3340(4) \times 10^{-16}$
F2, Spin-frequency derivative 2 ($\frac{\mathrm{Hz}}{\mathrm{s}^2}$)	$2.242(4) \times 10^{-25}$
F3, Spin-frequency derivative 3 ($\frac{\mathrm{Hz}}{\mathrm{s}^3}$)	$-3.44(5) \times 10^{-34}$
F4, Spin-frequency derivative 4 ($\frac{\mathrm{Hz}}{\mathrm{s}^4}$)	$-6.20(7) \times 10^{-42}$
F5, Spin-frequency derivative 5 ($\frac{\mathrm{Hz}}{\mathrm{s}^5}$)	$1.78(4) \times 10^{-50}$
F6, Spin-frequency derivative 6 ($\frac{\mathrm{Hz}}{\mathrm{s}^6}$)	$2.92(7) \times 10^{-58}$
DM, Dispersion measure ($\frac{\mathrm{pc}}{\mathrm{cm}^3}$)	241.713(5)
DM1, 1'th time derivative of the dispersion measure ($\frac{\mathrm{pc}}{\mathrm{yr\,cm}^3}$)	0.0610(5)
Set Quantities	
CHI2R, Reduced chi-squared value obtained during fitting	29.059610
TRES, TOA residual after fitting (μs)	458.996331
POSEPOCH, Reference epoch for position (d)	54054.849300
PEPOCH, Reference epoch for spin-down (d)	54054.849337
NE_SW, Solar Wind density at 1 AU ($\frac{1}{\mathrm{cm}^3}$)	10.000000
SWP, Solar Wind Model radial power-law index (only for SWM=1)	2.000000
DMEPOCH, Epoch of DM measurement (d)	54054.849337
PB, Orbital period (d)	0.075646
PBDOT, Orbital period derivative respect to time	-0.000000
A1, Projected semi-major axis of pulsar orbit, ap*sin(i) (ls)	0.119622
T0, Epoch of periastron passage (d)	47967.521151